Inorganic Chemistry

Article

pubs.acs.org/IC

Independent Control of Optical and Explosive Properties: Pyrazole–Tetrazine Complexes of First Row Transition Metals

Thomas W. Myers,*[,†] David E. Chavez,*[,†] Susan K. Hanson,[‡] R. Jason Scharff,[†] Brian L. Scott,[§] Jacqueline M. Veauthier,*[,‡] and Ruilian Wu[∥]

[†]M Division, [‡]Chemistry Division, [§]Materials Physics and Applications, and [∥]Bioscience Division, Los Alamos National Laboratory, P.O. Box 1663, Los Alamos, New Mexico 87545, United States

Supporting Information

ABSTRACT: Complexes of 3-amino-6-(3,5-dimethylpyrazole)-tetrazine) (NH_2TzDMP, **1**) and 3-(3,3′-dinitroazetidine)-6-(3,5-dimethylpyrazole)tetrazine) (DNAZTzDMP, **2**) with first row transition metal centers were synthesized. Reactions of $Fe^{II}(H_2O)_6(BF_4)_2$ and $Fe(NO_3)_3{\cdot}9H_2O$ with **1** and **2** both led to complexes of the form $[(RTzDMP)_3Fe]X_2$ (X = BF_4, R = NH_2 (**3**), DNAZ (**4**); X = NO_3, R = NH_2 (**5**), DNAZ (**6**)), which showed intense MLCT bands in the visible region of the spectrum. Ligands **1** and **2** also reacted with $Cu^{II}(NO_3)_2{\cdot}5/2H_2O$ to form $[(RTzDMP)_2Cu(NO_3)][NO_3]$ (R = NH_2 (**7**), DNAZ (**8**)) in addition to reacting with $Cu^{I}(CH_3CN)_4(PF_6)$ to form $[(RTzDMP)_2Cu][PF_6]$ (R = NH_2 (**9**), DNAZ (**10**)). Lastly reactions of **1** and **2** with $Co(NO_3)_2{\cdot}6H_2O$ and $Ni(NO_3)_2{\cdot}6H_2O$ led to $[(NH_2TzDMP)_2Co(H_2O)(NO_3)][NO_3]$ (**11**), $[(DNAZTzDMP)_2Co(H_2O)_2][NO_3]_2$ (**12**), $[(NH_2TzDMP)_3Ni][NO_3]_2$ (**13**), and $[(DNAZTzDMP)_2Ni(H_2O)_2][NO_3]_2$ (**14**). The complexes display rich electrochemical and photophysical properties that are unaffected by derivation with explosive groups.

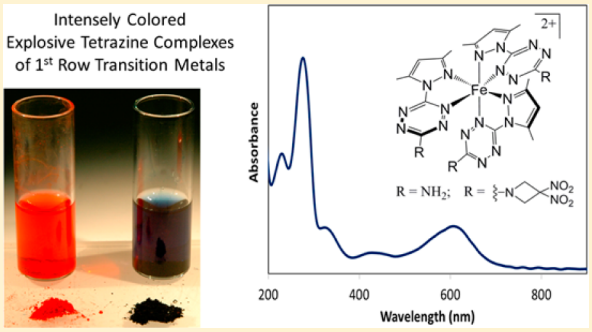

INTRODUCTION

The demand for safer high explosives (HE) that do not sacrifice performance has led to increased interest in alternate means of initiation. Photochemical and to a lesser extent electrochemical pathways to initiation could eliminate the need for HE with sensitivities to mechanical and thermal stimuli. Although some progress has been made toward optical initiation of energetic materials,[1] conventional explosives absorb weakly in the ultraviolet region of the electromagnetic spectra and do not absorb in the visible and near-infrared regions, limiting the efficiency of laser initiation.[2] Systems with optical and energetic properties that can be tuned independently are necessary to improve the efficiency of optical initiation.

In recent years, there has been growing interest in the synthesis of energetic coordination compounds (ECCs), in part due to the unique spectroscopic properties associated with inorganic complexes.[3] Metal tetrazole derivatives have been investigated as green primaries,[4] laser initiated primaries,[5] and material combustion synthesis precursors.[6] In general, metal tetrazole compounds display improved thermal stability and greater mechanical sensitivity compared to compounds with similar performance.[7] This could be due in part to their high nitrogen content, which in purely organic systems has been shown to lead to desirable sensitivity and performance properties.[8]

Nitrogen-rich tetrazine derivatives have been investigated as energetic materials due to their high nitrogen content, large positive heats of formation, low mechanical sensitivity, and high thermal stability.[9] Tetrazines have also been shown to have rich spectroscopic properties, including strong absorption of visible light, fluorescence, and reversible electrochemistry.[10] Tetrazines are readily derivatized with a variety of other high nitrogen groups[11] as well as traditional explosive groups, such as 3,3′-dinitroazetidine (DNAZ) and trinitropentaerythritol (PETrN).[12] This coupling of explosive groups to tetrazine has led to electroactive explosive chromophores.[13]

A number of nonexplosive metal tetrazine complexes have been reported by Kaim and co-workers, who examined the redox chemistry of Cu(I) metal centers complexed with neutral and radical 3,6-bis(2-pyridyl)-1,2,4,5-tetrazine (bptz) ligands.[14] In addition, Cu(I) centers with electron deficient tetrazine ligands have shown strong MLCT bands in the visible region of the spectra.[15] Similar charge transfer bands have been observed in Fe(II) complexes of pyridine-substituted tetrazine ligand complexes.[16] Tetrazine ligands with pyrazole substitution have also been studied for their propensity to form oligomers with a variety of transition metal centers.[17] We targeted the development of energetic metal tetrazine coordination compounds, as their rich spectroscopic properties could result in alternative initiation pathways. In addition, the ability to vary the metal center, energetic substituents on the tetrazine, and oxidizing anion employed should allow for enhanced control over the sensitivity and performance properties of the complexes.[3]

Received: June 10, 2015
Published: August 3, 2015

DOI: 10.1021/acs.inorgchem.5b01313
Inorg. Chem. 2015, 54, 8077–8086

Herein, we describe the synthesis and characterization of first row transition metal complexes of energetic tetrazine−pyrazole-based ligands. The optical properties of these complexes have been investigated, and both ligand centered (π to π^* and n to π^*) and metal-based (d to d and MLCT) transitions were observed. The replacement of an inert NH_2 group with an explosive DNAZ group on the tetrazine ligand does not fundamentally alter the optical properties of the resulting metal complexes, highlighting the ability to control the explosive properties independent of the optical properties.

RESULTS AND DISCUSSION

Syntheses and Spectroscopic Properties of Fe Complexes. To probe the effect that substitution of explosive groups has on the optical properties of metal tetrazine complexes, the ligands 3-amino-6-(3,5-dimethylpyrazole)-tetrazine) (NH_2TzDMP, **1**)[18] and 3-(3,3′-dinitroazetidine),6-(3,5-dimethylpyrazole)tetrazine) (DNAZTzDMP, **2**) were synthesized from 3,6-bis(3,5-dimethylpyrazole)tetrazine) (DMP_2Tz) through modified literature procedures (Scheme 1).[19] The amino group in **1** and the 3,3′-dinitroazetidine (DNAZ) in **2** have similar electronic properties but very different explosive properties.

Scheme 1. Synthesis of 1 and 2

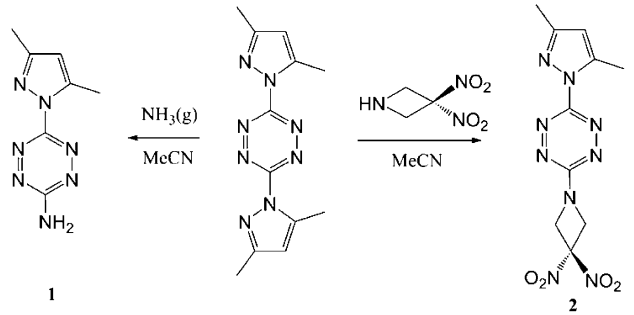

Initial efforts focused on the preparation of iron complexes of tetrazine ligands **1** and **2**, as several prior reports show that nonenergetic iron tetrazine complexes display strong metal-to-ligand charge transfer features in the optical spectrum.[16] The reaction between tetrazine **1** or **2** and $Fe^{II}(H_2O)_6(BF_4)_2$ proceeded rapidly at room temperature to form an intensely colored blue solution of $[(NH_2TzDMP)_3Fe][BF_4]_2$ (**3**) or $[(DNAZTzDMP)_3Fe][BF_4]_2$ (**4**) in 82 and 76% isolated yield, respectively (Scheme 2). In contrast to the reactions with iron(II) starting materials, which immediately formed dark blue complexes, reactions with the iron(III) precursor $Fe(NO_3)_3\cdot 9H_2O$ showed a fast color change, initially affording a brown solution that turned dark blue after 3 days. Attempts at isolating and characterizing the brown material were unsuccessful; however, $[(NH_2TzDMP)_3Fe][NO_3]_2$ (**5**) and $[(DNAZTzDMP)_3Fe][NO_3]_2$ (**6**) were isolated in 31 and 28% isolated yield, respectively, from the blue solution. Presumably upon complexation, the tetrazine ligand stabilizes the Fe(II) oxidation state, and an air stable Fe(II) complex is formed via reduction of the Fe(III) complex under ambient conditions. The exact reaction stoichiometry is somewhat unclear and may involve participation of the coordinated water in $Fe(NO_3)_3\cdot 9H_2O$ as a reducing agent. This was further supported by the electrochemistry of **3**−**6** (see below). Although no evidence of ligand oxidation products were observed in the ^{1}HNMR spectra of the reaction mixture, it cannot be ruled out as an alternate reaction pathway to **5** and **6**.

Scheme 2. Synthesis of Complexes 3−6

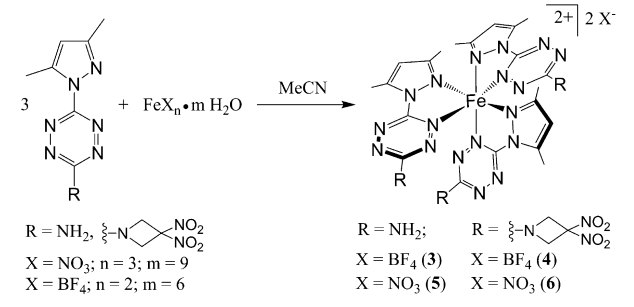

For the synthesis of **5** and **6** to be improved, magnesium was added as an external reducing agent. When the reactions were carried out in the presence of stoichiometric magnesium metal, the solution went from brown to blue in 30 min instead of 3 days. There was also a significant increase in the yields of **5** and **6** (from 31 and 28% to 71 and 62%, respectively). The results suggest that, upon coordination of **1** or **2** to an Fe center, the Fe^{II}/Fe^{III} redox couple is shifted to a positive enough potential to oxidize H_2O. However, the low yield of **5** and **6** in the absence of an external reductant suggests that **5** and **6** are not stable to the products of the H_2O oxidation.

Compounds **3**−**6** are all diamagnetic and display ^{1}HNMR spectra with peaks shifted downfield from the free ligands **1** and **2**. The UV−vis spectra of **3**−**6** each show strong ligand-based absorbances near 270, 330, and 420 nm in addition to a broad metal-to-ligand charge transfer band near 610 nm (Figure 1, Table S1). The presence of the DNAZ substitution in **4** and **6** has a negligible effect on the absorbance of the complexes relative to **3** and **5**. No d-d transitions could be resolved for complexes **3**−**6**.

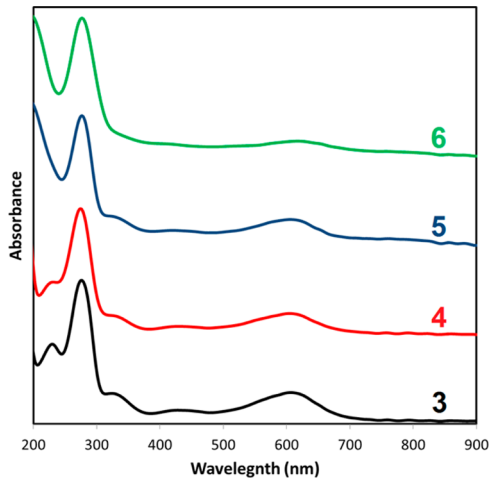

Figure 1. UV−vis spectra of **3** (black), **4** (red), **5** (blue), and **6** (green) in MeCN solution.

Solid-State Structures of Fe Complexes. Compounds **3**−**6** are octahedral complexes each containing 3 tetrazine ligands in a mer arrangement (Figure 2; Tables S2 and S5). The bite angle of the ligands is <90° in **3** (80.4(4)°), **4** (80.47(17)°), **5** (81.3(2)°), and **6** (80.78(10)°). This bite angle is the maximum deviation from ideal octahedral geometry in

DOI: 10.1021/acs.inorgchem.5b01313
Inorg. Chem. 2015, 54, 8077−8086

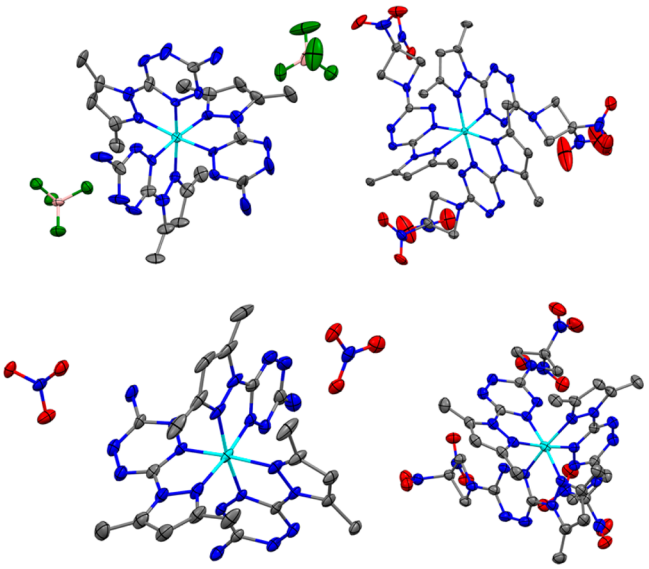

Figure 2. Solid-state structure of $[(NH_2TzDMP)_3Fe][BF_4]_2$ in **3** (upper left), $[DNAZTzDMP)_3Fe]^{2+}$ in **4** (upper right), $[NH_2TzDMP)_3Fe][NO_3]_2$ in **5** (lower left), and $[DNAZTzDMP)_3Fe]^{2+}$ in **6** (lower right). Cyan, red, pink, green, blue, and gray ellipsoids represent Fe, O, B, F, N, and C atoms, respectively. H atoms and solvent molecules have been omitted for clarity. Ellipsoids are at 40% probability.

3–**6**. The average metal–tetrazine distances in Fe(II) complexes **3**–**6** (1.857(8), 1.903(4), 1.903(3), and 1.900(2) Å, respectively) are shorter than the distances in other structurally characterized iron–tetrazine complexes.[16] In addition, the metal–tetrazine distances deviated <0.02 Å from each other in all four complexes, consistent with no Jahn–Teller distortions in low-spin d^6 complexes. The bond lengths and angles for the tetrazine ligands do not show significant deviation from those of the free ligand.[20] Although the bond lengths and angles in complexes of ligand **1** are very similar to those of complexes of ligand **2**, the C–N bond distance between the NH_2 group and the tetrazine ring in **1** is ~0.03 Å shorter than the C–N bond distance between the DNAZ group and the tetrazine ring in **2**.

Complexes **3** and **5** each displayed hydrogen bonding networks between the ligand NH_2 groups and the BF_4 and NO_3 counteranions. Complexes **4**–**6** exhibited close contacts between the counteranions and the tetrazine rings. The centroid F distance in **4** was 2.680(6) Å, whereas the centroid-O distance in **5** was 2.800(4) Å. Lastly, the nitrate anion in **6** is not centered above a single tetrazine ring but instead bridges between two rings with N–O distances of 2.852(4) and 2.866(5) Å. These anion-π interactions are common to metal tetrazine complexes due to the electron deficient nature of the tetrazine heterocycle.[21]

Syntheses and Spectroscopic Properties of Cu Complexes. The ability of the tetrazine ligands to stabilize lower oxidation states prompted us to investigate if other typically unstable oxidation states could be rendered air stable upon coordination. Toward this end, **1** and **2** were reacted with the copper salts $Cu^{II}(NO_3)_2{\cdot}5/2H_2O$ and $Cu^{I}(CH_3CN)_4(PF_6)$ (Scheme 3). Reaction of **1** or **2** with $Cu(NO_3)_2{\cdot}5/2H_2O$ afforded five coordinate complexes $[(NH_2TzDMP)_2Cu(NO_3)][NO_3]$ (**7**) and $[(DNAZTzDMP)_2Cu(NO_3)][NO_3]$ (**8**) in 91 and 79% isolated yield, respectively. In contrast to

Scheme 3. Synthesis of Complexes 7–10

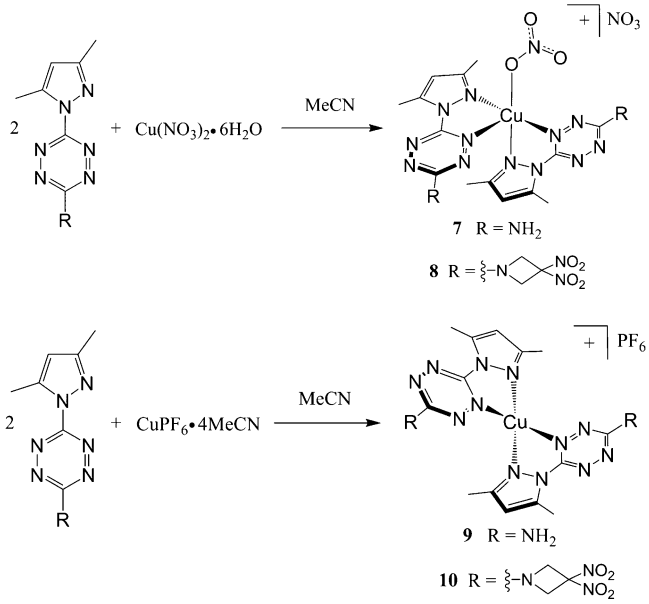

iron, which reacted with the tetrazine ligands in a 3:1 ligand/metal stoichiometry, copper(II) reacted with the tetrazine ligands to form complexes with a 2:1 ligand/metal stoichiometry. The difference in coordination number may be a consequence of the Jahn–Teller distortion associated with d^9 metal centers and the limited flexibility of ligands **1** and **2**.

The reactions with the copper(I) precursor $Cu^{I}(CH_3CN)_4(PF_6)$ led to the isolation of tetrahedral $[(NH_2TzDMP)_2Cu][PF_6]$ (**9**) and $[(DNAZTzDMP)_2Cu][PF_6]$ (**10**) in 91 and 88% yield, respectively. Complexes **9** and **10** are diamagnetic, and their ^{1}HNMR spectra exhibit minor resonance shifts compared to **1** and **2**. Both the Cu(I) and Cu(II) oxidation states are stable under ambient conditions. Furthermore, it is possible to reduce **7** and **8** to the corresponding Cu(I) species with ferrocene as a mild reductant.

There were no prominent MLCT bands observed in the UV–vis spectra of **7**–**10** in acetonitrile (Figure 3, Table S1).

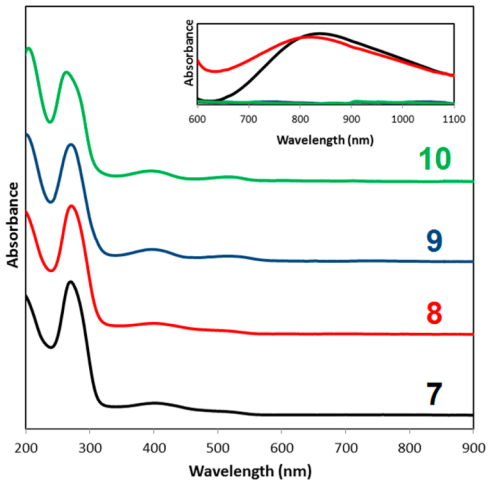

Figure 3. UV–vis spectra of **7** (black), **8** (red), **9** (blue), and **10** (green) in MeCN solution. Insert: UV–vis spectra of d-d transitions in **7** (black) and **8** (red) from 600 to 1100 nm.

DOI: 10.1021/acs.inorgchem.5b01313
Inorg. Chem. 2015, 54, 8077–8086

For Cu(II) complexes **7** and **8**, this was expected; however, previously reported copper(I) complexes of tetrazine ligands have shown MLCT bands in the NIR region of the electromagnetic spectrum.[15] In addition, compounds **9** and **10** were purple in the solid state but orange-brown in MeCN solution. To investigate this discrepancy, UV−vis spectra of **9** and **10** in the solid state were collected (Figure 4). In the solid

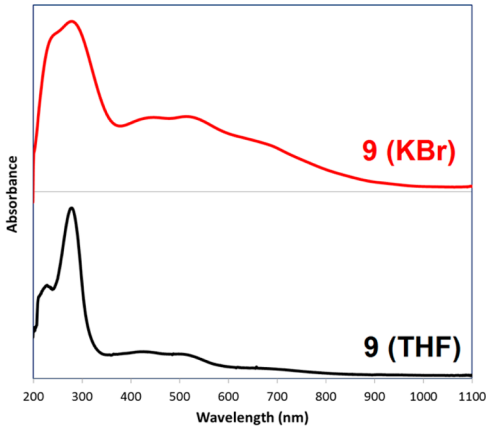

Figure 4. UV−vis spectra of **9** in THF solution (black) and in a solid-state KBr pellet (red).

state, complexes **9** and **10** exhibit broad MLCT bands at 690 nm. Similar MLCT bands were observed when the spectra were taken in THF but at lower relative intensity. A slight shift in the frequency and an increased intensity of the ligand-based π to π^* and n to π^* transitions was observed in the UV−vis spectra of **9** and **10**. In addition, d-d transitions for **7** and **8** were detected as exceedingly broad absorptions at 820 and 810 nm, respectively, typical of five coordinate Cu(II) complexes (Figure 3, insert).[22]

Solid-State Structures of Cu Complexes. Compounds **7** and **8** are five coordinate complexes with two bound ligands and one bound nitrate (Figure 5; Tables S3 and S6). The geometries are best described as distorted square pyramidal with τ_5 values of 0.211 and 0.222, respectively. Compounds **9** and **10** are each distorted tetrahedral complexes with τ_4 values of 0.750 and 0.574, respectively. The maximum deviation from ideal tetrahedral geometry in **9** is the angle between the tetrazine nitrogen of one ligand and the pyrazole nitrogen of the other ligand at 137.12(13)°, whereas the maximum deviation in **10** is the angle between the two pyrazole nitrogen atoms on different ligands at 140.7(3)°.

The metal tetrazine distances are 2.011(2) and 2.211(3) Å in **7** and 2.039(3) and 2.251(3) Åin **8**, clearly showing the Jahn−Teller distortion expected for a d^9 complex. The average metal pyrazole distance is 1.969(2) Å in **7** and 1.982(3) Å in **8**. No Jahn−Teller distortions are observed in **9** and **10** with less than 0.02 Å deviations in the metal−tetrazine and metal−pyrazole distances in both complexes.

Similar to complexes **3** and **5**, both complexes **7** and **9** have hydrogen bonding from the NH_2 group to the nitrate counteranion in **7** and the solvated ether in **9**. In addition, all four complexes have short contacts between the anions and the tetrazine rings. Complexes **7** and **8** have a short contact from the free nitrates with centroid O distances of 2.746(5) and 2.669(6) Å, respectively, along with a weaker interaction between the bound nitrate and the tetrazine ring with N−O distances of 3.002(7) and 3.028(7) Å, respectively. In **9** and **10**, the centroid F distances are 2.825(5) and 2.895(6) Å,

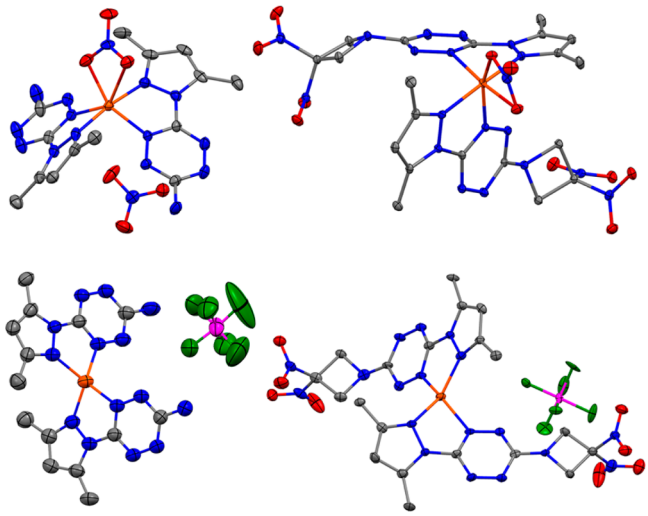

Figure 5. Solid-state structure of $[NH_2TzDMP)_2Cu(NO_3)][NO_3]$ in **7** (upper left), $[DNAZTzDMP)_2Cu(NO_3)]^+$ in **8** (upper right), $[NH_2TzDMP)_2Cu][PF_6]$ in **9** (lower left), and $[(DNAZTzDMP)_2Cu][PF_6]$ in **10** (lower right). Brown, green, magenta, red, blue, and gray ellipsoids represent Cu, F, P, O, N, and C atoms, respectively. H atoms and solvent molecules have been omitted for clarity. Ellipsoids are at 40% probability.

respectively. Lastly, complexes **9** and **10** also have π stacking interactions between the tetrazine rings, which may contribute to the differences in the solid-state and solution UV−vis spectra.

Syntheses and Spectroscopic Properties of Co and Ni Complexes. The coordination of tetrazines **1** and **2** with cobalt and nickel was investigated (Scheme 4). Reactions of **1** and **2** with $Co^{II}(NO_3)_2{\cdot}6H_2O$ led to octahedral complexes $[(NH_2TzDMP)_2Co(H_2O)(NO_3)][NO_3]$ (**11**) and

Scheme 4. Synthesis of Complexes 11−14

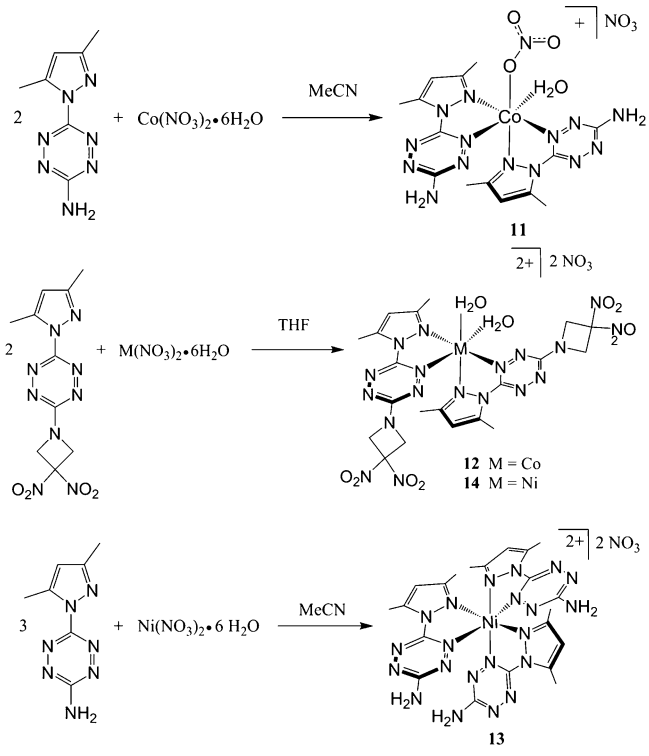

DOI: 10.1021/acs.inorgchem.5b01313
Inorg. Chem. 2015, 54, 8077−8086

$[(DNAZTzDMP)_2Co(H_2O)_2][NO_3]_2$ (**12**), respectively, in high yield (Scheme 3). Although both complexes coordinate only two tetrazine ligands, the lower steric demand of **1** allows for a nitrate ligand to remain in the coordination sphere of **11**, whereas the larger steric demand of **2** leads to the displacement of both nitrate anions by aqua ligands in **12**. Similarly, reactions of **1** and **2** with $Ni^{II}(NO_3)_2{\cdot}6H_2O$ led to octahedral complexes $[(NH_2TzDMP)_3Ni][NO_3]_2$ (**13**) and $[(DNAZTzDMP)_2Ni(H_2O)_2][NO_3]_2$ (**14**) (Figure 6). The smaller steric demand of **1** allows for three ligands to coordinate to the Ni(II) center in **13**.

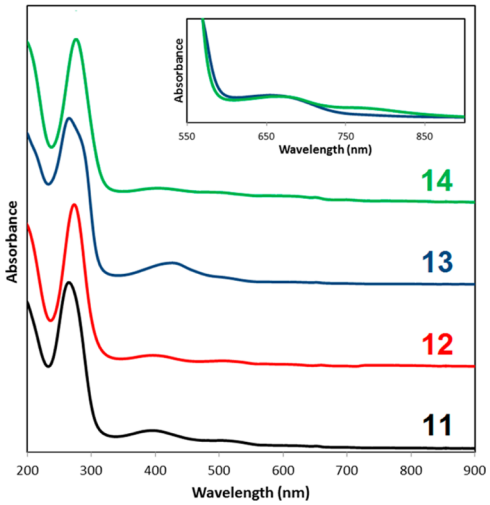

Figure 6. UV−vis spectra of **11** (black), **12** (red), **13** (blue), and **14** (green) in MeCN solution. Insert: UV−vis spectra of d-d transitions in **13** (blue) and **14** (green) from 550 to 900 nm.

Solid-State Structures of Co and Ni Complexes. Compounds **11**, **12**, and **14** have distorted octahedral geometries with only two ligands bound, whereas compound **13** has a distorted octahedral geometry with three ligands bound (Figures 7, 8; Tables S4 and S7). In **12** and **14**, water

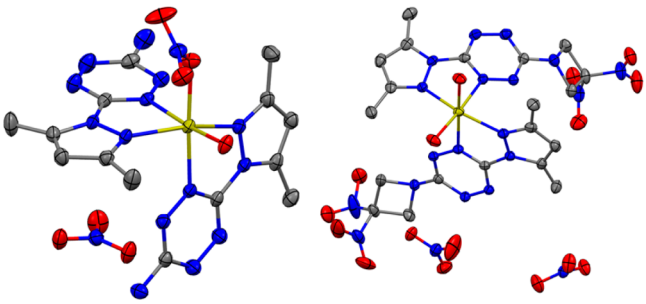

Figure 7. Solid-state structure of $[(NH_2TzDMP)_2Co(H_2O)(NO_3)][NO_3]$ in **11** (left) and $[(DNAZTzDMP)_2Co(H_2O)_2][NO_3]_2$ in **12** (right). Yellow, red, blue, and gray ellipsoids represent Co, O, N, and C atoms, respectively. H atoms and solvent molecules have been omitted for clarity. Ellipsoids are at 40% probability.

molecules occupy the remaining two sites, whereas in **11**, the remaining sites are occupied by one water molecule and one nitrate anion. Both complexes **5** and **13** and complexes **12** and **14** have similar connectivity, but are not isomorphous to each other. In **11**, **12**, and **13**, the bite angle of the ligands remains the greatest deviation from ideal octahedral geometry at 75.07(5)°, 74.65(11)°, and 77.62(11)°, respectively, whereas

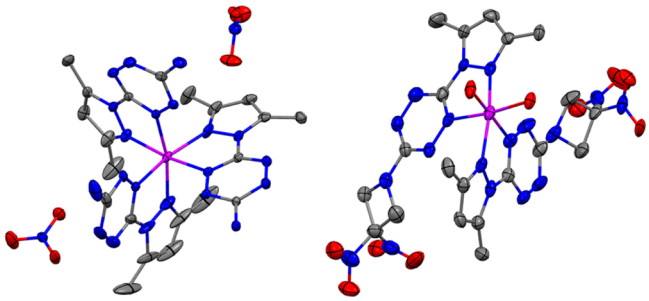

Figure 8. Solid-state structure of $[NH_2TzDMP)_3Ni][NO_3]_2$ in **13** (left) and $[DNAZTzDMP)_2Ni(H_2O)_2]^{2+}$ in **14** (right). Purple, red, blue, and gray ellipsoids represent Ni, O, N, and C atoms, respectively. H atoms, nitrate counteranions, and solvent molecules have been omitted for clarity. Ellipsoids are at 40% probability.

in **14**, the angle between the two water molecules (72.8(3)°) is more distorted than the ligand bite angle (76.3(3)°) in **14**. The increased steric demand of **2** compared to **1** is likely the cause of the distorted angles in **14** along with the different number of coordinated ligands as compared to **13**.

The metal−tetrazine distances (2.132(2) and 2.133(2) Å) and metal−pyrazole distances (2.109(2) and 2.118(2) Å) in **11** showed little deviation from each other. The metal−OH_2 and metal−ONO_2 distances were 2.045(2) and 2.129(2) Å, respectively. Complex **12** showed a slight tetragonal distortion with the metal−tetrazine and metal−OH_2 distances along one axis (2.182(3) and 2.067(3) Å, respectively) elongated compared to the other axis (2.139(3) and 2.029(3) Å, respectively). The two metal−pyrazole distances (2.103(3) and 2.133(3) Å) showed less deviation from each other. Complex **13** had an average metal−tetrazine distance of 2.074(4) Å and an average metal-pyrazole distance of 2.056(4) Å with no evidence of a Jahn−Teller distortion as expected for an octahedral d^8 complex. Lastly, complex **14** had significant tetragonal distortion with the metal−tetrazine and metal−OH_2 distances compressed along one axis (1.978(4) and 1.949(4) Å, respectively) compared to the other axis (2.122(4) and 2.106(4) Å, respectively). The metal-pyrazole distances were less distorted at 2.164(4) and 2.198(4) Å.

Complexes **11** and **13** both have hydrogen bonding between their NH_2 groups and the free nitrate counteranions. In addition, complexes **12**−**14** each have short contacts between the tetrazine rings and the counteranions. In **12** and **13**, the centroid O distances are 3.046(6) and 2.743(6) Å, respectively. In **14**, the nitrate counteranion bridges between two tetrazine rings with centroid O distances of 2.934(7) and 3.202(7) Å.

Thermal Stability and Mechanical Sensitivity. Complexes **6**, **8**, **10**, **12**, and **14** have calculated oxygen balances ranging from −70.6 to −83.3%, similar to TNT. Complex **4** has a lower oxygen balance of −102.9% due to the lack of an oxidizing anion (Table 1). Differential scanning calorimetry was performed at a 5 °C min^{-1} ramp rate on complexes **4**, **6**, **8**, **10**, **12**, and **14** to determine their thermal stability (Figures S13−S18). Complexes **6**, **10**, **12**, and **14** had thermal stabilities similar to PETN with decomposition beginning between 133 and 197 °C and peaking between 186 and 207 °C. Complex **4** is significantly more thermally stable with an onset of decomposition at 225 °C and peak decomposition occurring at 268 °C. This is most likely due to the nonoxidizing BF_4 counteranions. Complex **8** is significantly less thermally stable with an onset of 127 °C and a peak decomposition temperature

DOI: 10.1021/acs.inorgchem.5b01313
Inorg. Chem. 2015, 54, 8077−8086

Table 1. Sensitivity Properties of 4, 6, 8, 10, 12, and 14

	T_o (°C)[a]	T_p (°C)[b]	ρ (g/cm^3)[c]	Ω[d]	ID[e]	FD[f]	DDT[g]
4	225	268	1.554[h]	−102.9%	no	no	no
6	146	186	1.442[I]	−83.3%	yes	no	no
8	127	163	1.664[I]	−73.3%	yes	no	no
10	197	227	1.614	−82.8%	no	no	no
12	182	207	1.469[j]	−70.6%	yes	no	no
14	133	192	1.467[I]	−70.6%	yes	no	no

[a]Onset of decomposition temperature. [b]Peak of decomposition temperature. [c]Crystal density. [d]Oxygen balance: Ω = (−1600 (2(# of C atoms) + (# of H atoms)/2 + (# of M atoms) − (# of O atoms))/moleculer mass. [e]ID (impact detonation) while performing two hammer impact test. [f]FD (friction detonation) while performing hammer friction test. [g]DDT (deflagration-to-detonation transition) while performing flame test. [h]C_6H_{14} adduct. [I]MeCN adduct. [j]THF adduct.

of 162 °C. The presence of an inner sphere nitrate counteranion along with the ability of Cu to catalyze combustion when nitrate anions are present may contribute to the lower thermal stability of **8**.[3]

Complexes **4**, **6**, **8**, **10**, **12**, **14** were probed for their sensitivity to mechanical stimuli. Complexes **6**, **8**, **12**, and **14** were all sensitive toward impact, whereas complexes **4** and **10** were stable toward impact, most likely due to differences in the counteranions. In addition, none of the complexes displayed any sensitivity toward friction. Lastly, complexes **4**, **6**, **8**, **10**, **12**, and **14** did not detonate or deflagrate when exposed to flame. Overall, the complexes are relatively insensitive toward external stimuli as might be expected for such oxygen deficient complexes.

Although it was not practical to obtain quantitative sensitivity data for all six energetic complexes, complex **8** was identified as the most sensitive compound through the qualitative tests and was scaled to two grams for quantitative sensitivity measurements. Complex **8** was significantly less sensitive than PETN toward impact, friction, and spark (Table 2). The data are in good agreement with the qualitative sensitivity observations and suggest that each of the complexes is best considered a secondary explosive.

Table 2

	impact (J)[a]	spark (J)[b]	friction (N)[c]
8	51.6	0.125	>360
PETN	3.0	0.0625	91

[a]LANL type 12, 50% drop height, 2.5 kg using the Neyer D-Optical method. [b]ABL spark 3.4% threshold initiation level (TIL). [c]Fifty percent load determined using the Neyer D-Optical method.

Electrochemical Measurements. The electrochemical properties of **3**−**14** were investigated by cyclic voltammertry (CV) experiments performed in 0.1 M NBu_4PF_6 MeCN solutions. Iron complexes **3**−**6** all showed similar behavior (Figure 9, Table 3). Each complex showed three distinct reduction events from −0.40 to −1.18 V relative to Fc, likely corresponding to the reduction of each of the coordinated tetrazine ligands to the radical anion. The tetrazine reductions in the complexes are shifted more positive relative to those of **1** and **2** due to the stabilization provided by the divalent metal center. Similar behavior was reported previously by Kaim and co-workers for the iron complexes of the tetrazine derivative

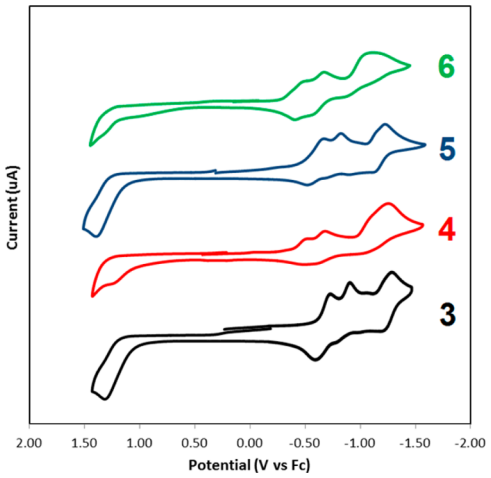

Figure 9. Cyclic voltammagrams of **3** (black), **4** (red), **5** (blue), and **6** (green) relative to Fc in 0.3 M $[Bu_4N][PF_6]$ MeCN solutions at a scan rate of 100 mV/s.

Table 3. Summary of Redox Events for 1−14

	$\Delta E_{1/2}$ (V vs Fc)			
1	−1.25			
2	−1.19			
3	1.27	−0.64	−0.84	−1.24
4	1.27	−0.46	−0.64	−1.01
5	1.33	−0.57	−0.77	−1.18
6	1.18	−0.45	−0.67	−1.05
7	0.34	−0.64		
8	0.40	−0.69		
9	0.33	−0.62		
10	0.46	−0.70		
11	−0.43			
12	−0.40	−0.62		
13	−0.57			
14	−0.52			

3,6-bis(2-pyridyl)-1,2,4,5-tetrazine) (btzp),which displays 3 tetrazine reductions between −0.190 and −0.850 V relative to Ag/AgCl.[16] In addition to the reductions, all four iron complexes show an oxidation event between 1.18 and 1.33 V relative to Fc, corresponding to the Fe^{II}/Fe^{III} couple. The highly anodic potential of the Fe^{II}/Fe^{III} couple is consistent with prior observations that ligands with higher nitrogen content have more anodic Fe^{II}/Fe^{III} couples.[23] The extreme potential of the Fe^{II}/Fe^{III} couple also supports the assignment of water as the reducing agent in the formation of **5** and **6** in the absence of an external reductant. This was further probed by running cyclic voltammagrams in the presence of added water (Figure 10). Additions of 0.5, 1.0, and 1.5 equiv of H_2O to a solution of **5** each led to an increase in relative current, indicating that oxidation is occurring. Addition of further equiv of H_2O led to a decrease in current and a disappearance of the couples associated with the reductions of **5**, likely due to the decomposition of **5**. These observations are consistent with the proposed formation of **5** from $Fe(NO_3)_3{\cdot}9H_2O$ and **1**.

Copper complexes **7**−**10** all showed similar electrochemical behavior to each other (Figure 11). Complexes **7**−**10** each display a redox couple ranging from 0.25 to 0.41 V corresponding to the Cu^I/Cu^{II} couple. Similar to the potential of the Fe^{II}/Fe^{III} couple, the anodic shift of the Cu^I/Cu^{II} couple can likely be explained by the high nitrogen electron deficient

DOI: 10.1021/acs.inorgchem.5b01313
Inorg. Chem. 2015, 54, 8077−8086

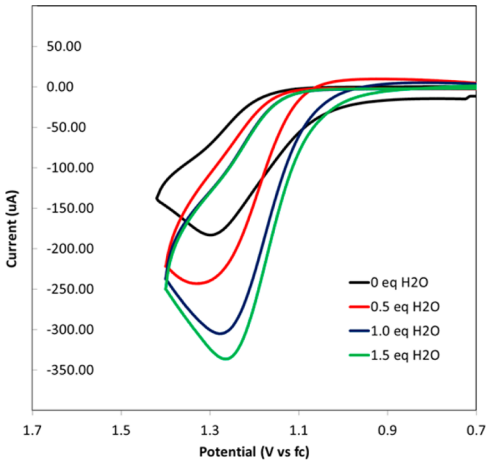

Figure 10. Cyclic voltammagrams of **5** with 0 (black), 0.5 (red), 1.0 (blue), and 1.5 (green) equiv of H_2O relative to Fc in 0.3 M $[Bu_4N][PF_6]$ MeCN solutions at a scan rate of 100 mV/s.

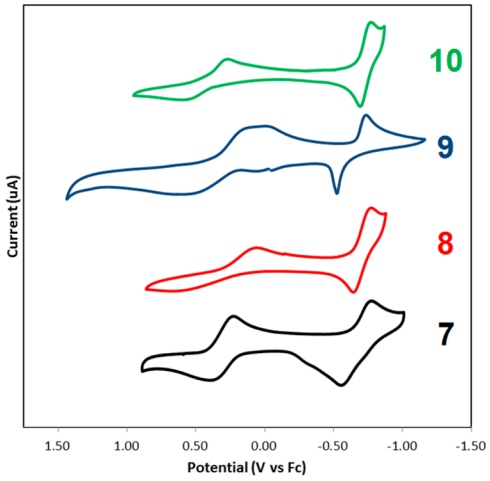

Figure 11. Cyclic voltammagrams of **7** (black), **8** (red), **9** (blue), and **10** (green) in 0.3 M $[Bu_4N][PF_6]$ MeCN solutions at a scan rate of 100 mV/s.

tetrazine ligand leading to an air stable copper(I) complex. In addition, all four complexes show a single irreversible reduction event between −0.62 and −0.72 V relative to Fc. Although this reduction could be attributable to either the reduction of one of the tetrazine ligands to the radical anion or to the Cu^I/Cu^0 couple, the reduction is likely ligand based because no stable complexes of Cu^0 have been isolated to date.[16d] In addition, the presence of an MLCT band in complexes **9** and **10** suggests that the event is likely a tetrazine reduction because the MLCT transition involves the formal oxidation of the metal and reduction of the ligand. Lastly, similar behavior is observed in copper complexes of bis(tetrazine)pyridine, which has a Cu^I/Cu^{II} redox couple at 0.500 V relative to Ag/AgCl and a tetrazine reduction at −0.450 V relative to Ag/AgCl.[16d]

Co (II) and Ni (II) complexes **11**−**14** showed redox behavior that was more difficult to assign (Figure 12). The cyclic voltammagram of complex **12** shows two redox events at −0.40 and −0.62 V relative to Fc, which can be assigned to the stepwise reduction of each of the tetrazine ligands to the radical anion. Complexes **11**, **13**, and **14**, however, only had a single reduction at −0.43, −0.52, and −0.57 V relative to Fc, respectively. The consistency of the potential of the redox

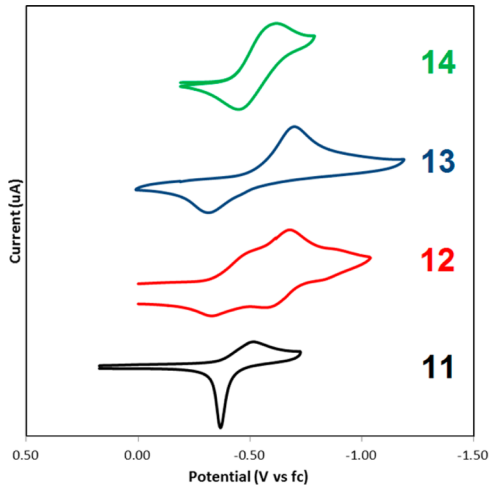

Figure 12. Cyclic voltammagrams of **11** (black), **12** (red), **13** (blue), and **14** (green) in 0.3 M $[Bu_4N][PF_6]$ MeCN solutions at a scan rate of 100 mV/s.

couple in **11**, **13**, and **14** with not only themselves but also with the first tetrazine reduction in complexes **3**−**6** suggests that the couple is tetrazine based. However, this is not consistent with the presence of only one observable reduction because each complex has at least two tetrazine ligands. At significantly more negative potentials, there are additional irreversible redox events, further suggesting that the electrochemistry of these complexes are more complex than that of the corresponding Fe and Cu complexes. No oxidations were observed within the solvent window for **11**−**14**. Overall, all the Fe, Cu, Co, and Ni complexes showed a variety of reversible metal- and ligand-based reductions at potentials that were relatively unaffected by substitution of explosive for inert groups.

CONCLUSIONS AND OUTLOOK

We have demonstrated the synthesis of complexes of nonenergetic and energetic pyrazole−tetrazine ligands with late first row transition metal centers. To our knowledge, these are the first tetrazine-based energetic coordination complexes that have been synthesized. Reactions of pyrazole tetrazine ligands with either Fe(II) or Fe(III) starting materials lead to the formation of deeply blue Fe(II) octahedral complexes. The color of these complexes is the result of intense MLCT bands, which are unaffected by the replacement of the inert NH_2 groups with the explosive DNAZ group. The iron complexes display rich electrochemistry with an Fe^{II}/Fe^{III} redox couple at a highly anodic potential and three quasi-reversible tetrazine reductions at mild potentials.

We have also demonstrated that pyrazole tetrazine ligands react with Cu(II) and Cu(I) starting materials to form 5 coordinate Cu(II) and tetrahedral Cu(I) complexes. The Cu(II) complexes have a brown appearance due to strong tetrazine-based absorptions along with weaker Cu-based d-d transitions. The Cu(I) complexes are purple in the solid state due to a strong MLCT band that decreases in relative intensity in polar solvents. Again, the absorption spectra of these Cu−tetrazine complexes are unaffected by substitution of explosive groups on the ligands. The complexes share similar electrochemical behavior with a quasi-reversible Cu^I/Cu^{II} couple and a quasi-reversible tetrazine reduction at mild potentials.

Lastly, pyrazole−tetrazine ligands also form octahedral complexes with Co(II) and Ni(II) metal centers. No MLCT

DOI: 10.1021/acs.inorgchem.5b01313
Inorg. Chem. 2015, 54, 8077−8086

bands are observed in either case, and while the d-d transitions can be resolved for the Ni(II) complexes, they cannot be resolved for the Co(II) complexes. The complexes show greater variety in coordination environment with either two or three ligands coordinating along with a variable number of inner sphere water molecules and nitrate counteranions depending on the steric demand of the ligand employed. The complexes also display complicated electrochemical behavior. Although the Co(II) complexes of inert and explosive tetrazines show little difference in their absorption spectra, the Ni(II) complex of the inert tetrazine has a single d-d transition whereas the Ni(II) complex of the explosive tetrazine has two d-d transitions. This is most likely due to the greater steric demand of the explosive tetrazine, which leads to fewer coordinated ligands and lower symmetry.

Overall, there are few differences in the optical and electronic properties of complexes of the nonenergetic and energetic ligands, demonstrating that the energetic and optical properties can be tuned independently of each other. This independent control can lead to explosives that are not only optimized for sensitivity and performance, but also tunable to wavelengths that coincide with commercially available laser sources. Future work will focus on utilizing ligands with better oxygen balance to improve the explosive properties as well as investigating other ligand metal combinations for absorption in different regions of the visible spectrum.

EXPERIMENTAL SECTION

Caution! *Although no problems occurred during the synthesis and handling of these complexes, the materials are explosive. Laboratories and personnel should be properly grounded and safety equipment, such as Kevlar gloves, blast shields, and ear plugs, are necessary, especially when working with large scale reactions.*

Physical Measurements. Elemental analyses for **3**, **7**, **9**, **11**, and **13** were performed by Atlantic Microlab, Inc. of Norcross, GA. Elemental analyses for all other complexes were performed using a PerkinElmer series II 2400 CHNS/O analyzer. Elemental analysis of explosive compounds often returns low values for the N%, and materials were purified until satisfactory C% and H% values were obtained.[24] ^{1}HNMR spectra were recorded at ambient temperature using a Bruker Avance 400 MHz spectrometer. Chemical shifts (δ) were referenced to the residual solvent signal. Electrochemical measurements were recorded under a dinitrogen atmosphere using a CHI electrochemical analyzer, a glassy carbon working electrode, a Pt wire auxiliary electrode, and a $Ag/AgNO_3$ nonaqueous reference electrode. Reported potentials are all referenced to the Fc/Fc^+ couple and were determined using ferrocene as an internal standard. Unless noted otherwise, UV−vis spectra were recorded in MeCN solutions using an HP 8453 Agilent UV−vis spectrometer. Differential scanning calorimetry was performed using a TA Instruments 2920 Modulated DSC at 5 °C/min heating ramp rate.

X-ray Structure Determinations. X-ray diffraction studies were carried out on a Bruker APEX II equipped with a CCD area detector or on a Rigaku R-axis IV with an imaging plate detector. Measurements were carried out at −173 °C using Mo Kα 0.71073 radiation. Crystals were mounted on a Kaptan loop with paratone-N oil. Initial lattice parameters were obtained from a least-squared analysis of more than 100 centered reflections; these parameters were later refined against all data. Data were integrated and corrected for Lorentz polarization effects using SAINT[25] and were corrected for absorption effects using SADABS 2.3.[26]

Space group assignments were based upon systematic absences, E statistics, and successful refinement of the structures. Structures were solved by direct methods with the aid of successive difference Fourier maps and were refined against all data using the SHELXTL 5.0 software package.[27] Thermal parameters for all non-hydrogen atoms were refined anisotropically. Hydrogen atoms, where added, were assigned to ideal positions and refined using a riding model with an isotropic thermal parameter 1.2 times that of the attached carbon atom (1.5 times for methyl hydrogens).

Sensitivity Tests. Qualitative hammer tests were performed by placing ∼10 mg of dry compound on a 6″ × 6″ × 2″ steel block. The material was gently compressed with a ball peen hammer and a second hammer was used to strike the material with increasing impact strength until decomposition of the material was observed. If no amount of impact could induce decomposition of the material, it was deemed insensitive. Qualitative friction tests were performed by placing 10 mg of dry material on a 6″ × 6″ × 2″ steel plate. The material was compressed between the steel plate and a ball peen hammer. The hammer was dragged across the face of the steel plate at various intensities. If no amount of friction could cause decomposition of the material, it was deemed insensitive. Qualitative flame tests were performed by placing ∼10 mg of dry material on the end of a metal scoopula behind a blast shield. The material was heated with a long neck butane lighter until it decomposed. DDT was characterized by the rapid combustion of the material in conjunction with an audible detonation.

Quantitative impact sensitivity tests were performed on a LANL type 12 instrument with a 50% drop height and a 2.5 kg weight using the Neyer D-Optimal method. Quantitative friction sensitivity tests were performed with a BAM friction instrument determining the 50% load using the Neyer D-Optimal method. Quantitative electrostatic discharge sensitivity testing was performed on an ABL ESD instrument.

Preparation of Compounds. Deuterated solvents were purchased from Cambridge Isotopes Laboratories, Inc. and used without purification. The compounds 3-amino-6-(3,5-dimethylpyrazole)-tetrazine (**1**) and DNAZ·HCl were synthesized according to a literature procedure.[12a,18] All other reagents were purchased from commercial vendors and used without further purification.

*DNAZTzDMP (**2**).* To a solution of DMP_2Tz (2.72 g, 10.0 mmol) in MeCN (10 mL) were added DNAZ·HCl (1.83 g, 10.0 mmol) and triethylamine (1.11 g, 11.0 mmol). The resulting solution was stirred for 1 h until the color had changed to a uniform orange-red color. Diethyl ether (20 mL) was added, and the precipitate was collected via filtration. The precipitate was washed with water (3 × 10 mL) and diethyl ether (2 × 10 mL). Recrystallization of the crude material from MeCN led to isolation of DNAZTzDMP (**2**, 2.50 g, 78%) as orange-red crystals. ^{1}HNMR (400 mHz, d_6-DMSO): δ 2.24 (s, 3H, CH_3), 2.46 (s, 3H, CH_3), 5.28 (s, 4H, DNAZ), 6.26 (s, 1H, pyr). ^{13}CNMR (400 mHz, d_6-DMSO): δ 12.67 (CH_3), 13.37 (CH_3), 59.71 (DNAZ), 107.95 (DNAZ), 109.50 (pyr), 141.88 (pyr), 151.10 (pyr), 157.71 (tz), 162.58 (tz). Anal. Calcd (%) for $C_{10}H_{11}N_9O_4$: C, 37.39; H, 3.45; N, 39.24. Found: C, 37.73; H, 3.42; N, 38.89.

*$[(NH_2TzDMP)_3Fe][BF_4]_2$ (**3**).* To a solution of **1** (0.191 g, 1.00 mmol) in MeCN (5 mL) was added $Fe(BF_4)_2{\cdot}6H_2O$ (0.133 g, 0.334 mmol). The solution turned dark blue within seconds of the addition, and the resulting solution was stirred for an additional 30 min to ensure complete reaction. Solvent was removed in vacuo until 2 mL of MeCN remained, then diethyl ether (2 mL) was added to precipitate $[(NH_2TzDMP)_3Fe][BF_4]_2$ (**3**, 0.220 g, 82%) as a dark blue powder. Single crystals suitable for X-ray diffraction were grown by cooling a concentrated MeCN solution at 0 °C for 2 days. ^{1}HNMR (400 mHz, d_3-MeCN): δ 6.74 (s, 2H, NH_2), 6.49 (s, 1H, Pyr-H), 2.82 (s, 3H, CH_3), 1.79 (s, 3H, CH_3). UV−vis spectrum (MeCN) λ_{max} (ε_M): 276 (82,630), 334 (15,940), 434 (6,500), 611 (br, 16,670) nm (L mol^{-1} cm^{-1}). Anal. Calcd (%) for $C_{21}H_{27}B_2F_8FeN_{21}$: C, 31.41; H, 3.39; N, 36.63. Found: C, 31.08; H, 3.70; N, 35.10.

*$[(DNAZTzDMP)_3Fe][BF_4]_2$ (**4**).* To a solution of **2** (0.321 g, 1.00 mmol) in THF (5 mL) was added $Fe(BF_4)_2{\cdot}6H_2O$ (0.133 g, 0.334 mmol). The solution turned dark blue within seconds of the addition, and the resulting solution was stirred for an additional 30 min to ensure complete reaction. Hexane (5 mL) was added to precipitate $[(NH_2TzDMP)_3Fe][BF_4]_2$ (**4**, 0.254 g, 76%) as a dark blue powder. Single crystals suitable for X-ray diffraction were grown by cooling a concentrated MeCN solution at 0 °C for 2 days. ^{1}HNMR (400 mHz, d_6-acetone): δ 6.70 (s, 1H, pyrazole), 5.13 (s, 4H, DNAZ), 2.91 (s,

DOI: 10.1021/acs.inorgchem.5b01313
Inorg. Chem. 2015, 54, 8077−8086

6H, CH_3). UV−vis spectrum (MeCN) λ_{max} (ε_M): 277 (80,420), 331 (13,520), 427 (6,240), 607 (br, 14,510) nm (L mol^{-1} cm^{-1}). Anal. Calcd (%) for $C_{30}H_{33}B_2F_8FeN_{27}O_{12}$: C, 30.20; H, 2.79; N, 31.69. Found: C, 30.07; H, 2.86; N, 30.87.

*[(NH$_2$TzDMP)$_3$Fe][NO$_3$]$_2$ (**5**).* (Method A) To a solution of **1** (0.191 g, 1.00 mmol) in MeCN (5 mL) was added $Fe(NO_3)_3{\cdot}9H_2O$ (0.134 g, 0.333 mmol). The initial dark yellow solution was stirred for 3 days until it was a uniform deep blue color. The solvent was reduced in vacuo until 2 mL of MeCN remained. Then, diethyl ether (2 mL) was added, and the solution was cooled to 0 °C overnight. The dark blue precipitate was collected via filtration and recrystallized from a concentrated MeCN solution. [(NH$_2$TzDMP)$_3$Fe][NO$_3$]$_2$ (**5**, 0.084 g, 31%) was collected as dark blue crystals suitable for single crystal diffraction. ^{1}HNMR (400 mHz, d_6-acetone): δ 7.00 (s, 2H, NH_2), 6.59 (s, 1H, Pyr-H), 2.92 (s, 3H, CH_3), 1.89 (s, 3H, CH_3). UV−vis spectrum (MeCN) λ_{max} (ε_M): 272 (79,120), 333 (15,470), 432 (7,960), 609 (br, 13,810) nm (L mol^{-1} cm^{-1}). Anal. Calcd (%) for $C_{21}H_{27}FeN_{23}O_6$: C, 33.48; H, 3.61; N, 42.75. Found: C, 33.80; H, 3.89; N, 41.46.

*[(NH$_2$TzDMP)$_3$Fe][NO$_3$]$_2$ (**5**).* (Method B) To a solution of **1** (0.191 g, 1.00 mmol) in MeCN (5 mL) was added $Fe(NO_3)_3{\cdot}9H_2O$ (0.134 g, 0.333 mmol) and magnesium (0.004 g, 0.167 mmol). The solution was stirred and within 5 min turned a dark blue color. The solution was stirred at room temperature for an additional 2 h. Diethyl ether (10 mL) was added to precipitate a dark blue solid product. The dark blue precipitate was collected by filtration and recrystallized from a concentrated MeCN solution. Dark blue crystals of **5** (0.193g, 71%) were collected via filtration and characterized by ^{1}HNMR spectroscopy, which matched the previously obtained spectra for **5**.

*[(DNAZTzDMP)$_3$Fe][NO$_3$]$_2$ (**6**).* To a solution of **2** (0.321 g, 1.00 mmol) in MeCN (5 mL) was added $Fe(NO_3)_3{\cdot}9H_2O$ (0.134 g, 0.333 mmol) and magnesium (0.0040 g, 0.17 mmol). The solution was stirred and within 5 min was a dark blue color. The solution was stirred at room temperature for an additional 2 h. The solution was concentrated to a volume of ∼1 mL of MeCN under vacuum, and then, diethyl ether (3 mL) was added to precipitate [(DNAZTzDMP)$_3$Fe][NO$_3$]$_2$ (**6**, 0.196 g, 62%) as a dark blue powder. Crystals suitable for single crystal X-ray diffraction were grown from the slow diffusion of diethyl ether into a concentrated MeCN solution at 0 °C overnight. ^{1}HNMR (400 mHz, d_6-acetone): δ 6.21 (s, 1H, pyrazole), 5.46 (s, 4H, DNAZ), 2.93 (s, 6H, CH_3). UV−vis spectrum (MeCN) λ_{max} (ε_M): 276 (78,050), 334 (14,770), 415 (6,660), 620 (13,310) nm (L mol^{-1} cm^{-1}). Anal. Calcd (%) for $C_{30}H_{33}FeN_{29}O_{18}$: C, 31.51; H, 2.91; N, 35.52. Found: C, 31.85; H, 2.65; N, 35.21.

*[(NH$_2$TzDMP)$_2$Cu][NO$_3$]$_2$ (**7**).* To a solution of **1** (0.191 g, 1.00 mmol) in MeCN (5 mL) was added $Cu(NO_3)_2{\cdot}2.5H_2O$ (0.116 g, 0.500 mmol). The orange solution was stirred at room temperature for 15 min until it was a uniform brown color. The solution was concentrated to 2 mL, and diethyl ether (10 mL) was added to precipitate [(NH$_2$TzDMP)$_2$Cu][NO$_3$]$_2$ (7, 0.259 g, 91%) as a brown powder. Single crystals suitable for X-ray diffraction were grown from a concentrated MeCN solution at 0 °C over 3 days. UV−vis spectrum (MeCN) λ_{max} (ε_M): 271 (47,960), 404 (6,540), 511 (2,090), 820 (br, 270) nm (L mol^{-1} cm^{-1}). Anal. Calcd (%) for $C_{14}H_{18}CuN_{16}O_6$: C, 29.51; H, 3.18; N, 39.32. Found: C, 29.73; H, 3.57; N, 38.86.

*[(DNAZTzDMP)$_2$Cu][NO$_3$]$_2$ (**8**).* To a solution of **2** (0.321 g, 1.00 mmol) in MeCN was added $Cu(NO_3)_2{\cdot}2.5H_2O$ (0.116 g, 0.500 mmol). The resulting yellow-brown solution was stirred for 30 min to ensure complete reaction. Diethyl ether (20 mL) was added to precipitate [(DNAZTzDMP)$_2$Cu][NO$_3$]$_2$ (**8**, 0.277 g, 79%). Crystals suitable for single crystal X-ray diffraction were grown by the slow diffusion of diethyl ether into a concentrated MeCN solution at 0 °C. UV−vis spectrum (MeCN) λ_{max} (ε_M): 275 (49,280), 394 (6,060), 519 (2,100), 810 (br, 250) nm (L mol^{-1} cm^{-1}). Anal. Calcd (%) for $C_{20}H_{22}CuN_{20}O_{14}{\cdot}C_2H_3N$: C, 30.20; H, 2.87; N, 33.77. Found: C, 30.16; H, 2.88; N, 34.12.

*[(NH$_2$TzDMP)$_2$Cu][PF$_6$] (**9**).* To a solution of **1** (0.191 g, 1.00 mmol) in THF (5 mL) was added [Cu(MeCN)$_4$][PF$_6$] (0.186 g, 0.500 mmol). The orange solution was stirred at room temperature for 15 min until it was a uniform purple color. The solution was concentrated to 2 mL, and hexane (10 mL) was added to precipitate [(NH$_2$TzDMP)$_2$Cu][PF$_6$] (**9**, 0.270 g, 91%) as a purple powder. Single crystals suitable for X-ray diffraction were grown from a concentrated MeCN solution at 0 °C over 3 days. ^{1}HNMR (400 mHz, d_6-acetone): δ 6.86 (s, 2H, NH_2), 6.45 (s, 2H, Pyr-H), 2.71 (s, 3H, CH_3), 2.33 (s, 3H, CH_3). UV−vis spectrum (MeCN) λ_{max} (ε_M): 273 (47,450), 401 (6,510), 509 (3,000) nm (L mol^{-1} cm^{-1}). Anal. Calcd (%) for $C_{14}H_{18}CuF_6N_{14}P$: C, 28.08; H, 3.03; N, 32.74. Found: C, 27.76; H, 3.34; N, 32.95.

*[(DNAZTzDMP)$_2$Cu][PF$_6$] (**10**).* To a solution of **2** (0.321 g, 1.00 mmol) in MeCN (5 mL) was added [Cu(MeCN)$_4$][PF$_6$] (0.186 g, 0.500 mmol). The resulting brown solution was stirred for 30 min. Diethyl ether (20 mL) was added to precipitate [(DNAZTzDMP)$_2$Cu][PF$_6$] (**10**, 0.318 g, 88%) as a brown powder. Crystals suitable for single crystal X-ray diffraction were grown by cooling a concentrated MeCN solution at 0 °C for 3 days. ^{1}HNMR (400 mHz, d_6-acetone): δ 6.42 (s, 1H, Pyr-H), 5.37 (s, 4H, CH_2), 2.79 (s, 3H, CH_3), 2.41 (s, 3H, CH_3). UV−vis spectrum (MeCN) λ_{max} (ε_M): 270 (48,810), 397 (5,720), 520 (2,550) nm (L mol^{-1} cm^{-1}). Anal. Calcd (%) for $C_{20}H_{22}CuF_6N_{18}O_8P{\cdot}C_4H_8O$: C, 31.77; H, 3.31; N, 27.80. Found: C, 31.60; H, 3.43; N, 27.70.

*[(NH$_2$TzDMP)$_2$(H$_2$O)$_2$Co][NO$_3$]$_2$ (**11**).* To a solution of **1** (0.191 g, 1.00 mmol) in MeCN (5 mL) was added $Co(NO_3)_2{\cdot}6H_2O$ (0.145 g, 0.500 mmol). The orange solution was stirred at room temperature for 15 min until it was a uniform dark brown color. The solution was concentrated to 2 mL, and diethyl ether (10 mL) was added to precipitate [(NH$_2$TzDMP)$_2$(H$_2$O)$_2$Co][NO$_3$]$_2$ **11** (0.257 g, 83%) as a brown powder. Single crystals suitable for X-ray diffraction were grown from a concentrated MeCN solution at 0 °C over 3 days. UV−vis spectrum (MeCN) λ_{max} (ε_M): 267 (48,770), 395 (5,130), 507 (2,280) nm (L mol^{-1} cm^{-1}). Anal. Calcd (%) for $C_{14}H_{20}CoN_{16}O_7$: C, 28.83; H, 3.46; N, 38.42. Found: C, 28.63; H, 3.58; N, 38.09.

*[(DNAZTzDMP)$_2$Co(H$_2$O)$_2$][NO$_3$]$_2$ (**12**).* To a solution of **2** (0.321 g, 1.00 mmol) in THF (5 mL) was added $Co(NO_3)_2{\cdot}6H_2O$ (0.145 g, 0.500 mmol). The resulting orange-brown solution was stirred for an additional 30 min to ensure complete reaction. Hexane (10 mL) was added to precipitate [(DNAZTzDMP)$_2$Co(H$_2$O)$_2$][NO$_3$]$_2$ (**12**, 0.327 g, 77%) as a brown powder. Single crystals suitable for X-ray diffraction were grown by the slow diffusion of hexane into a concentrated THF solution at 0 °C. UV−vis spectrum (MeCN) λ_{max} (ε_M): 272 (47,340), 402 (5,010), 509 (2,550) nm (L mol^{-1} cm^{-1}). Anal. Calcd (%) for $C_{20}H_{26}CoN_{20}O_{16}$: C, 27.88; H, 3.04; N, 32.52. Found: C, 28.13; H, 2.86; N, 32.24.

*[(NH$_2$TzDMP)$_3$Ni][NO$_3$]$_2$ (**13**).* To a solution of **1** (0.191 g, 1.00 mmol) in MeCN (5 mL) was added $Ni(NO_3)_2{\cdot}6H_2O$ (0.097 g, 0.333 mmol). The initially orange solution was stirred at room temperature for 15 min until it turned a uniform yellow-brown color. The solution was concentrated to 2 mL and diethyl ether (10 mL) was added to precipitate [(NH$_2$TzDMP)$_3$Ni][NO$_3$]$_2$ **13** (0.199 g, 79%) as a yellow powder. Single crystals suitable for X-ray diffraction were grown from a concentrated MeCN solution at 0 °C over 3 days. UV−vis spectrum (MeCN) λ_{max} (ε_M): 268 (78,780), 428 (10,560), 510 (3,690), 660 (90) nm (L mol^{-1} cm^{-1}). Anal. Calcd (%) for $C_{21}H_{27}N_{23}NiO_6$: C, 33.36; H, 3.60; N, 42.59. Found: C, 33.38; H, 3.86; N, 42.26.

*[(DNAZTzDMP)$_2$Ni(H$_2$O)$_2$][NO$_3$]$_2$ (**14**).* To a solution of **2** (0.321 g, 1.00 mmol) in THF (5 mL) was added $Ni(NO_3)_2{\cdot}6H_2O$ (0.097 g, 0.33 mmol). The yellow solution was stirred for 30 min to ensure complete reaction. Hexane (10 mL) was added to precipitate [(DNAZTzDMP)$_2$Ni(H$_2$O)$_2$][NO$_3$]$_2$ (**14**, 0.310 g, 72%) as a yellow brown powder. Single crystals suitable for X-ray diffraction were grown by cooling a concentrated THF solution at 0 °C over 1 week. UV−vis spectrum (MeCN) λ_{max} (ε_M): 278 (47,960), 409 (5,220), 499 (3,740), 670 (85), 775 (65) nm (L mol^{-1} cm^{-1}). Anal. Calcd (%) for $C_{22}H_{30}N_{20}NiO_{16.5}$ (compound analyzed as 0.5 THF adduct): C, 29.45; H, 3.37; N, 31.22. Found: C, 29.53; H, 3.01; N, 31.42.

DOI: 10.1021/acs.inorgchem.5b01313
Inorg. Chem. 2015, 54, 8077−8086

■ ASSOCIATED CONTENT

Supporting Information

The Supporting Information is available free of charge on the ACS Publications website at DOI: 10.1021/acs.inorgchem.5b01313.

UV−vis tables, crystallographic data, and DSC plots (PDF)

CIF file (CIF)

■ AUTHOR INFORMATION

Corresponding Authors

*E-mail: twmyers@lanl.gov.

*E-mail: dechavez@lanl.gov.

*E-mail: veauthier@lanl.gov.

Funding

This work was supported by Los Alamos National Laboratory LDRD (20150005DR) and by a Director's Postdoctoral Fellowship for T.W.M.

Notes

The authors declare no competing financial interest.

■ ACKNOWLEDGMENTS

We also thank G. Brown, A. M. Giambra, S. I. Hagelberg, and M. Sandstrom for assistance with CHN and DSC analysis.

■ REFERENCES

(1) (a) Bowden, M. D.; Cheeseman, M.; Knowles, S. L.; Drake, R. C. *Proceedings of the SPIE* **2007**, *6662*, 08. (b) Kunz, A. B.; Kuklja, M. M.; Botcher, T. R.; Russell, T. P. *Thermochim. Acta* **2002**, *384*, 279−284. (c) Greenfield, M.; Guo, Y. Q.; Bernstein, E. R. *Chem. Phys. Lett.* **2006**, *430*, 277−281. (d) Bhattacharya, A.; Bernstein, E. R. *J. Phys. Chem. A* **2011**, *115*, 4135−4147.

(2) Aluker, E. D.; Krechetov, A. G.; Mitrofanov, A. Y.; Zverev, A. S.; Kuklja, M. M. *J. Phys. Chem. C* **2012**, *116*, 24482−24486.

(3) Sinditskii, V. P.; Serushkin, V. V. *Def. Sci. J.* **1996**, *46*, 371.

(4) (a) Huynh, M. H. V.; Coburn, M. D.; Meyer, T. J.; Wetzler, M. *Proc. Natl. Acad. Sci. U. S. A.* **2006**, *103*, 10322−10327. (b) Huynh, M. H. V.; Hiskey, M. A.; Meyer, T. J.; Wetzler, M. *Proc. Natl. Acad. Sci. U. S. A.* **2006**, *103*, 5409−5412.

(5) (a) Fischer, D.; Klapötke, T. M.; Piercey, D. G.; Stierstorfer, J. *J. Energ. Mater.* **2012**, *30*, 40−54. (b) Fischer, N.; Joas, M.; Klapötke, T. M.; Stierstorfer, J. *Inorg. Chem.* **2013**, *52*, 13791−13802. (c) Joas, M.; Klapötke, T. M.; Szimhardt, N. *Eur. J. Inorg. Chem.* **2014**, *2014*, 493−498. (d) Evers, J.; Gospodinov, I.; Joas, M.; Klapötke, T. M.; Stierstorfer, J. *Inorg. Chem.* **2014**, *53*, 11749−11756.

(6) (a) Tappan, B. C.; Huynh, M. H. V.; Hiskey, M. A.; Chavez, D. E.; Luther, E. P. *J. Am. Chem. Soc.* **2006**, *128*, 6589−6594. (b) Tappan, B. C.; Steiner, S. A., III; Luther, E. P. *Angew. Chem., Int. Ed.* **2010**, *49*, 4544−4565.

(7) (a) Tao, G.-H.; Twamley, B.; Shreeve, J. M. *Inorg. Chem.* **2009**, *48*, 9918−9923. (b) Tao, G.-H.; Parrish, D. A.; Shreeve, J. M. *Inorg. Chem.* **2012**, *51*, 5305−5312. (c) Joas, M.; Klapötke, T. M.; Stierstorfer, J.; Szimhardt, N. *Chem. - Eur. J.* **2013**, *19*, 9995−10003. (d) Huber, S.; Izsák, D.; Karaghiosoff, K.; Klapötke, T. M.; Reuter, S. *Propellants, Explos., Pyrotech.* **2014**, *39*, 793−801.

(8) (a) Christe, K. O. *Propellants, Explos., Pyrotech.* **2007**, *32*, 194. (b) Klapotke, T. M.; Sabate, C. M. *Chem. Mater.* **2008**, *20*, 3629. (c) Ye, C.; Gao, H.; Boatz, J. A.; Drake, G. W.; Twamley, B.; Shreeve, J. M. *Angew. Chem., Int. Ed.* **2006**, *45*, 7262.

(9) (a) Chavez, D. E.; Hiskey, M. A.; Naud, D. L. *Propellants, Explos., Pyrotech.* **2004**, *29*, 209−215. (b) Chavez, D. E.; Tappan, B. C.; Hiskey, M. A.; Son, S. F.; Harry, H. H.; Montoya, D.; Hagelberg, S. *Propellants, Explos., Pyrotech.* **2005**, *30*, 412−417. (c) Chavez, D. E.; Hiskey, M. A.; Gilardi, R. D. *Angew. Chem., Int. Ed.* **2000**, *39*, 1791−1793.

(10) Clavier, G.; Audebert, P. *Chem. Rev.* **2010**, *110*, 3299.

(11) (a) Chavez, D. E.; Gilardi, R. D. *J. Energ. Mater.* **2009**, *27*, 110−117. (b) Licht, H.-H.; Ritter, H. *J. Energ. Mater.* **1994**, *12*, 223−235. (c) Duddu, R.; Dave, P. R.; Damavarapu, R.; Surapaneni, R.; Gilardi, R.; Parrish, D. *Synth. Commun.* **2008**, *38*, 767−774. (d) Huynh, M. H. V.; Hiskey, M. A.; Archuleta, J. G.; Roemer, E. L.; Gilardi, R. *Angew. Chem., Int. Ed.* **2004**, *43*, 5658−5661. Chavez, D. E.; Gilardi, R. D. *J. Energ. Mater.* **2009**, *27*, 110−117.

(12) (a) Hiskey, M. A.; Johnson, M. C.; Chavez, D. E. *J. Energ. Mater.* **1999**, *17*, 233−254. (b) Chavez, D. E.; Hiskey, M. A. *J. Energ. Mater.* **1999**, *17*, 357−377. (c) Lee, K.-Y.; Storm, C. B.; Hiskey, M. A.; Coburn, M. D. *J. Energ. Mater.* **1991**, *9*, 415−428.

(13) Chavez, D. E.; Hanson, S. K.; Veauthier, J. M.; Parrish, D. A. *Angew. Chem., Int. Ed.* **2013**, *52*, 6876−6879.

(14) (a) Kaim, W.; Kohlmann, S. *Inorg. Chem.* **1987**, *26*, 1470−1472. (b) Schwach, M.; Hausen, H.-D.; Kaim, W. *Inorg. Chem.* **1999**, *38*, 2242−2243. (c) Glöckle, M.; Hübler, K.; Kümmerer, H.-J.; Denninger, G.; Kaim, W. *Inorg. Chem.* **2001**, *40*, 2263−2269.

(15) McNitt, K. A.; Parimal, K.; Share, A. I.; Fahrenbach, A. C.; Witlicki, E. H.; Pink, M.; Bediako, D. K.; Plaisier, C. L.; Le, N.; Heeringa, L. P.; Griend, D. A. V.; Flood, A. H. *J. Am. Chem. Soc.* **2009**, *131*, 1305.

(16) (a) Ketterle, M.; Fiedler, J.; Kaim, W. *Chem. Commun.* **1998**, 1701−1702. (b) Glöckle, M.; Kaim, W. *Inorg. Chem.* **1999**, *38*, 3270−3274. (c) Glöckle, M.; Katz, N. E.; Ketterle, M.; Kaim, W. *Inorg. Chim. Acta* **2002**, *336*, 55−60. (d) Benson, C. R.; Hui, A. K.; Parimal, K.; Cook, B. J.; Chen, C. − H.; Lord, R. L.; Flood, A. H.; Caulton, K. G. *Dalton Trans.* **2014**, *43*, 6513−6524.

(17) (a) Eremenko, I. L.; Malkov, A. E.; Sidorov, A. A.; Fomina, I. G.; Aleksandrov, G. G.; Nefedov, S. E.; Rusinov, G. L.; Chupakhin, O. N.; Novotortsev, V. M.; Ikorskii, V. N.; Moiseev, I. I. *Inorg. Chim. Acta* **2002**, *334*, 334−342. (b) Malkov, A. E.; Fomina, I. G.; Sidorov, A. A.; Aleksandrov, G. G.; Egorov, I. M.; Latosh, N. I.; Chupakhin, O. N.; Rusinov, G. L.; Rakitin, Y. V.; Novotortsev, V. M.; Ikorskii, V. N.; Eremenko, I. L.; Moiseev, I. I. *J. Mol. Struct.* **2003**, *656*, 207−224. (c) Cherdantseva, E. V.; Starichenko, D. V.; Slepukhin, P. A.; Ishmetova, R. I.; Shvachko, Y. N.; Korolev, A. V.; Rusinov, G. L.; Ustinov, V. V.; Matern, A. I.; Charushin, V. N. *Russ. Chem. Bull.* **2010**, *59*, 703−709.

(18) Chavez, D. E.; Hiskey, M. A. *J. Heterocycl. Chem.* **1998**, *35*, 1329−1332.

(19) Hiskey, M. A.; Johnson, M. C.; Chavez, D. E. *J. Energ. Mater.* **1999**, *17*, 223−254.

(20) Nayak, A.; Patra, S.; Sarkar, B.; Ghumaan, S.; Puranik, V. G.; Kaim, W.; Lahiri, G. K. *Polyhedron* **2005**, *24*, 333−342.

(21) (a) Dunbar, K. R.; Chifotides, H. T. *Acc. Chem. Res.* **2013**, *46*, 894−906. (b) Schottel, B. L.; Chifotides, H. T.; Shatruk, M.; Chouai, A.; Pèrez, L. M.; Bacsa, J.; Dunbar, K. R. *J. Am. Chem. Soc.* **2006**, *128*, 5895−5912.

(22) Rossi, A. R.; Hoffmann, R. *Inorg. Chem.* **1975**, *14*, 365−374.

(23) Cook, L. J. K.; Tuna, F.; Halcrow, M. A. *Dalton Trans.* **2013**, *42*, 2254−2265.

(24) Swift, H. *Microchem. J.* **1966**, *11*, 193.

(25) *SMART Software Users Guide*, version 5.1; Bruker Analytical X-Ray Systems, Inc.: Madison, WI, 1999.

(26) *SAINT Software Users Guide*, version 7.0; Bruker Analytical X-Ray Systems, Inc.: Madison, WI, 1999.

(27) Sheldrick, G. M. *SADABS*, version 2.03; Bruker Analytical X-Ray Systems, Inc.: Madison, WI, 2000.

DOI: 10.1021/acs.inorgchem.5b01313
Inorg. Chem. 2015, 54, 8077−8086